Forest Ecology and Management 543 (2023) 121137

Contents lists available at ScienceDirect

Forest Ecology and Management

journal homepage: www.elsevier.com/locate/foreco

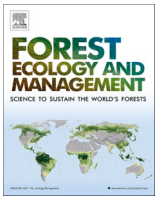

Modelling height growth of temperate mixedwood forests using an age-independent approach and multi-temporal airborne laser scanning data

José Riofrío [a,*], Joanne C. White [b], Piotr Tompalski [b], Nicholas C. Coops [a], Michael A. Wulder [b]

[a] Integrated Remote Sensing Studio, Department of Forest Resources Management, University of British Columbia, 2424 Main Mall, Vancouver, BC V6T 1Z4, Canada
[b] Canadian Forest Service (Pacific Forestry Centre), Natural Resources Canada, 506 West Burnside Road, Victoria, BC V8Z 1M5, Canada

ARTICLE INFO

Keywords:
Multi-temporal ALS
Temperate mixedwood forest
Height growth model
Age-independent
Forest inventory

ABSTRACT

Forest inventories provide information regarding the status of a range of attributes as well as enabling predictive applications. Growth and yield models are essential tools for sustainable forest management, importantly enabling projections of future forest conditions (such as height growth). To select the most appropriate growth trajectory, site index models are commonly used to quantify the productivity of a given site. However, applying these methods to more complex, multi-species, and multi-age forests can be challenging due to deviations from the assumptions made for even-aged stands. In this study, we provide a comprehensive indicator of site quality for more complex and irregular stand structures by developing age-independent height growth models for various forest types. We used multi-temporal airborne laser scanning (ALS) data from 2005, 2012, and 2018 in the Great Lakes–St. Lawrence forest region in southern Ontario, Canada. The stochastic differential equations approach was used to develop age-independent height models and a height growth rate index as a proxy of site quality from ALS-derived height metrics. We evaluated the sensitivity of the models using two different modelling approaches and found that the model that incorporated data from both periods (i.e., 2005–2012 and 2012–2018) generally provided the lower root mean square error (RMSE) value for most forest types. Overall, our results showed good agreement between the model predictions of top height and observed top height in 2018 from field plots for all forest types. We demonstrated the use of these models by creating a system of height growth curves for each forest type and producing a map of site quality for a mixedwood forest (~10,000 ha) at a spatial resolution of 25 m. The approach developed herein leverages the accurate, spatially detailed characterization of canopy heights afforded by ALS data and is independent of stand age, which is challenging to measure accurately and is typically not available at a spatial resolution that is commensurate with the ALS data. Additionally, the demonstrated approach can be adapted to other data sources that accurately capture canopy heights (i.e., digital aerial photogrammetric or DAP), thereby increasing the possible geographic extent of height growth estimates.

1. Introduction

The characterization of forest growth is key information needed for a broad range of forest management decisions. Growth and yield (G&Y) models are a critical tool to determine sustainable timber yield, examine the efficacy of silvicultural strategies, and assess forest growth over time. Typical stand-level models predict stand volume, basal area or biomass as a function of age, site index (SI), and stand density (Weiskittel et al., 2011). Estimates of site quality are a key component of G&Y models and are a crucial requirement in the sustainable management of forest resources, with height growth and site index models as the most popular tools to quantify and classify the productivity of a site (Bravo et al., 2019). Top height of a stand at a specified reference age is often used as a common expression of site quality because height growth is highly correlated with stand volume or biomass productivity, and top height is not greatly affected by stand density or thinning treatments (Pretzsch, 2009; Weiskittel et al., 2011). While definitions of top height or stand dominant height vary (Zhou et al., 2019), the concept of top height is intended to characterize the average height of a specific number or proportion of the largest trees in a stand, typically the mean height of the 100 largest diameter trees per hectare (Rennolls, 1978).

The SI concept was developed for even-aged stands (Skovsgaard and

* Corresponding author.
E-mail address: jriofrio@mail.ubc.ca (J. Riofrío).

https://doi.org/10.1016/j.foreco.2023.121137
Received 11 January 2023; Received in revised form 17 May 2023; Accepted 19 May 2023
Available online 1 June 2023

Vanclay, 2008) based on three fundamentals: (1) site classification by stand height, (2) Eichhorn's rule describing the relationship between total growth and stand height (Assmann, 1970), and (3) the thinning response hypothesis, which posits that stand volume growth is generally not significantly affected by thinning for a wide range of thinning grades or stocking densities. However, applying SI to more complex multi-species and multi-age forests is not straightforward because the basic assumptions for site index are not met (del Río et al., 2016; Pretzsch and Zenner, 2017). For instance, due to inter-specific interactions, the relationship between total yield and top height in mixed stands can deviate from what might be expected for monospecific stands (Toïgo et al., 2015). Moreover, in multilayered uneven-aged stands, age is not easily available from inventory or monitoring data (del Río et al., 2016) and tree social status is not always fixed over time (Pretzsch, 2021).

Various methods have been proposed for developing height growth and SI for mixed and uneven-aged stands. For instance, integrating measures of stand structure in the G&Y models themselves (Anyomi et al., 2014) or using a SI conversion equation approach that estimate SI of one species from the SI of another has been applied for mixed stands (Nigh, 2002). However, because these methods are based on height-age models developed for even-aged monospecific stands, caution is advised in their application because, for a given site and age, the interaction between species could alter the height–age relationship and thereby bias SI estimates (del Río et al., 2016; Weiskittel et al., 2011). Site form index, defined as the dominant height of the stand at a reference dominant diameter (Vanclay and Henry, 1988), has been used for estimating site quality for different stand structures (even- and uneven-aged). Although this method might generate similar performance for estimating site quality compared with a traditional height-age SI in even-aged stands (Molina-Valero et al., 2019), the application to more complex forest structures might be constrained due to the inherent sensitivity of diameter growth to stand density (Wang, 1998; Weiskittel et al., 2011). Especially in mixed-species stands where stand density can alter diameter growth dynamics (Condés et al., 2013; Garber and Maguire, 2004). The need for an indicator for site productivity in mixedwoods or multi-aged forests has been addressed by the application of indices relying on past stand basal area or biomass increments (Berrill and O'Hara, 2014; Hennigar et al., 2017) or by developing geocentric methods that use edaphic, physiographic or climatic information for quantifying site quality (Dănescu et al., 2017).

Finding a comprehensive indicator of site productivity for more complex and irregular stand structures remains a fundamental concern in forestry (Berrill and O'Hara, 2014; Dănescu et al., 2017; Hennigar et al., 2017). Using a top height growth model as a site productivity indicator for those types of forest structures requires three basic properties: (1) been independent of age structure, (2) providing a reliable representation of the site productivity level, and (3) being able to capture the possible effects of stand composition and structure in height growth along environmental gradients (Berrill and O'Hara, 2014; del Río et al., 2016).

Airborne laser scanning (ALS) provides accurate estimates of forest structure attributes, such as canopy height, aboveground biomass, and volume distributions, and has demonstrated utility in improving the accuracy and resolution of forest inventories at the individual tree- and stand-level (Enhanced Forest Inventories - EFI) (Andersen et al., 2006; White et al., 2017). The increasing availability of multi-temporal ALS data can potentially characterize changes in forest attributes on a broad spatial scale (Dalponte et al., 2019; McRoberts et al., 2015; Tompalski et al., 2021; Zhao et al., 2018). The integration of spatially explicit forest attributes generated from ALS data has the potential to improve G&Y projections (Fekety et al., 2015; Lamb et al., 2018; Tompalski et al., 2016), for instance, by enabling spatially explicit estimates of site quality from a single (Tompalski et al., 2022), bi-, or multi-temporal ALS acquisitions (Noordermeer et al., 2020; Socha et al., 2017). While there is increasing availability of multi-temporal ALS data, bi-temporal ALS data is more widely available to characterize changes in forest attributes on a broad spatial scale (McRoberts et al., 2015; Riofrío et al., 2022; Tompalski et al., 2021). However, the impact of using bi- or multi-temporal ALS series to estimate changes in forest attributes, i.e., height increments, has been less explored (but see Hopkinson et al., 2008) and a comprehensive assessment of different approaches and data inputs is necessary.

Recent studies have demonstrated the application of the generalized algebraic difference approach (GADA) (Cieszewski and Bailey, 2000) to develop age-independent height growth and site index models for monospecific dominant, even-aged stands using bi-temporal ALS data (Guerra-Hernández et al., 2021; Solberg et al., 2019). Recently, a promising approach derived from stochastic differential equations (SDE) (García, 1983) was proposed by Salas-Eljatib (2020), who developed age-independent height growth and SI models adapted to complex forest structures where no single meaningful age is required. Advantages of the approach include the capability to project height growth to different period lengths without interpolating the predictions and the inclusion of a stochastic term in the error structure of the formulation that accounts for the uncertainty associated with height trajectories over time as a result of underlying, unknown processes (i.e., environmental-noise; García, 1983; Rennolls, 1995).

The diverse temperate mixedwood forests of the Great Lakes–St. Lawrence forest region in southern Ontario, Canada is located in a transition zone between boreal forests dominated by coniferous species to the north and deciduous-dominated temperate hardwood forests to the south. Several SI models are available throughout Ontario and incorporated into G&Y models (Sharma et al., 2008). More recent efforts have focused on incorporating the effects of climate on the tree height growth/site index models for plantations (Sharma and Parton, 2019) and mixed stands (Sharma, 2022, 2021). However, the need for models to evaluate site quality for mixedwoods and uneven or multi-aged stand structures remains (Carmean et al., 2013; Penner and Pitt, 2019; Sharma et al., 2008).

In this study, we hypothesize that by using the ability of multi-temporal ALS data to accurately quantify height increments and a stochastic differential equations approach, it is feasible to develop age-independent top height growth models and a growth-rate index as a proxy of site quality for complex forest structures typical of the Great Lakes–St. Lawrence forest region. Our objectives were to 1) develop age-independent height growth models using height increments derived from multi-temporal ALS data (a height growth rate index); 2) evaluate the sensitivity of the models to two different modelling approaches (i.e., periods); 3) validate the prediction capability of the height growth models using an independent data set; and finally 4) use the derived growth-rate index to map site quality of mixedwood forest at high spatial precision (25 m) for forest planning and management purposes.

2. Materials and methods

2.1. Study area

This study was conducted in the Petawawa Research Forest (PRF) which occupies approximately 10,000 ha of a diverse temperate mixedwood forest (Fig. 1). PRF is a continuously operated research forest that hosts different silvicultural field studies, intensive forest management interventions, plantations, and genetic trials (White et al., 2019). Coniferous dominant tree species in the area include jack pine (*Pinus banksiana* Lamb.), white pine (*Pinus strobus* L.), red pine (*Pinus resinosa* Ait.), white spruce (*Picea glauca* (Moench) Voss), and eastern hemlock (*Tsuga canadensis* L.), while deciduous species include trembling aspen (*Populus tremuloides* Michx), sugar maple (*Acer saccharum* Marsh), red maple (*Acer rubrum* L.), red oak (*Quercus rubra* L.), and white birch (*Betula papyrifera* Marsh). Species diversity and long-term silviculture history characterize the structural complexity of stands in the PRF, combining experimental plots, plantations, and long-term management plans (White et al., 2019).

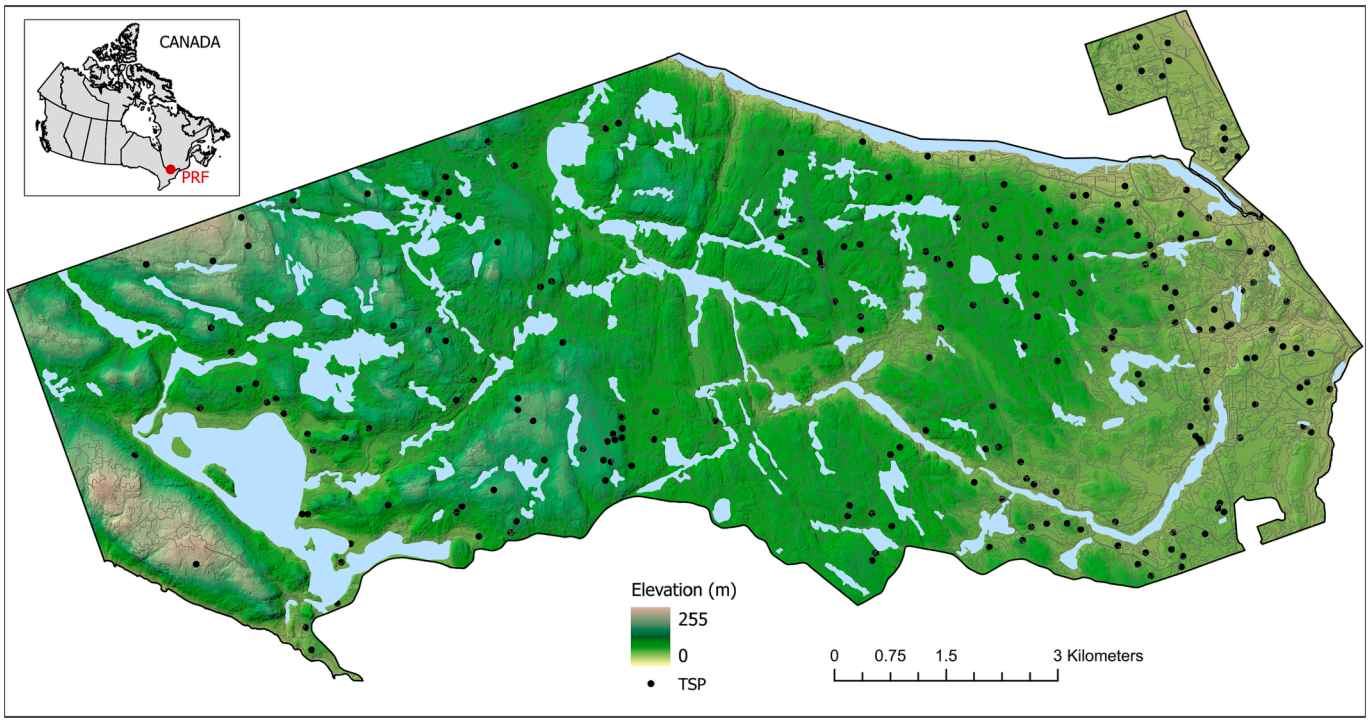

Fig. 1. Petawawa Research Forest is located in the Great Lakes–St. Lawrence forest region in southern Ontario, Canada. Field sample plots (TSP) were distributed throughout the research forest.

We gathered auxiliary information on stand attributes from the most up-to-date forest resources inventory available for the PRF, which was updated circa 2018. The inventory contains manually delineated forest stand polygons (n = 3072) defined via interpretation of digital aerial imagery and considering geographic features and homogeneity of forest cover and vegetation (Ontario Ministry of Natural Resources and Forestry, 2009). Stand polygons include attributes of overstory, species composition, vertical structure, silvicultural interventions, management type, and year of origin, among others. We used the stand species composition to define forest groups based on the dominant species in the canopy (Table 1).

2.2. Field sample plots

A total of 175 field sample plots (TSP) (14.1 m radius, 625 m^2) were established in 2012 and remeasured in 2018 (Fig. 1), covering the full range of species composition and stand development stages, following a structurally guided sampling approach (White et al., 2013). The plot locations were remeasured in 2018 using a TopCon™ GPS unit and post-processed using the Canadian Spatial Reference System Precise Point Positioning Tool (Natural Resources Canada 2020). All stems greater than 9.1 cm in diameter were measured for diameter at breast height over bark (DBH). Tree height was measured using a Haglof™ Vertex hypsometer for a subsample of trees (free from any visible top damage), with the four largest diameter trees of the dominant species and the two largest diameter trees of the codominant species measured at each plot. We found missing height measures for at least one of the six thickest trees in 68% of the plots in 2012 and 56% in 2018. Therefore, missing tree heights were imputed based on generalized height–diameter models fitted for each species (Riofrío et al., 2022). Top height (H_{TOP}) was calculated as the average height of the six thickest trees per plot, except for managed and unmanaged natural pine stands (PW in Table 1), wherein H_{TOP} was calculated as the average height of the two thickest trees per plot. At PRF, a uniform shelterwood silvicultural system is frequently applied to natural and managed pine stands, leaving a few large trees remaining in the stand following harvesting interventions. In these shelterwood stands, H_{TOP} may be biased when heights of these tall residual trees are combined with the heights of the trees in the main canopy, which also results in an overestimation bias in height from the ALS data (White et al., 2021a). Stand-level variables were calculated from tree measurements and aggregated, considering the same forest type classification as the forest inventory (Table 2).

2.3. ALS data harmonization and derived height increments

ALS data were acquired in 2005, 2012 and 2018 during leaf-on periods. Table 3 details the different acquisition specifications regarding vertical datum, spatial referencing, and point density. The point density was highest for the ALS_{2018} data with 32 points m^{-2}, 12 points m^{-2} for ALS_{2012}, and lowest for ALS_{2005} with 0.5 points m^{-2}. To ensure consistency among the ALS datasets, harmonization of the ALS acquisitions was conducted based on assessing the planimetric and vertical alignment among all three datasets (Riofrío et al., 2022). The harmonization consisted of projecting all ALS datasets to UTM Zone 18 N and transforming them to same vertical datum using the ALS_{2012} as reference (CGVD28). The vertical alignment based on the elevation reference model applied to all ALS acquisitions minimize errors in derived height increments (Riofrío et al., 2022). Digital terrain models (DTM) were generated for each ALS dataset using returns classified as 'ground'. Control points were located along roads distributed throughout the PRF to quantify the average elevation difference between DTMs. A total of 4183 control points (with a minimum of 50 m between points) were used for comparison. The ALS_{2012} data were selected as the reference for harmonization based on assessing the quality of PRF terrain models (DTM) (White et al., 2021b). Point clouds were adjusted using the average difference values calculated from the road point reference analyses and were all tiled using the same tiling scheme (i.e., 1 × 1 km tiles, no buffers, and the same naming convention). Finally, we used the 2012 reference DTM at 1 m resolution from ground-classified returns to normalize point cloud heights to heights above ground level.

We used the harmonized ALS point clouds to calculate height and height increments using an area-based approach (ABA), which estimates

Table 1
Description of forest types defined based on forest inventory species composition in the overstory. Height (H_{TOP}) and total height increment (H_{TOP} increment) were calculated based on the mean ALS-derived 99th percentile at stand polygon level (minimum and maximum values in parenthesis). H_{TOP} increment values correspond to the period 2005–2018.

Forest type	N stands	Area (ha)	H_{TOP} (m)	Total H_{TOP} increment (m)	Description
White Spruce (SW)	138	105.2	15.99 (0.04 – 32.00)	4.66 (−3.79–11.11)	Planted white spruce stands with various initial densities and subsequent management activities, in some cases with an understory of poplar and hardwoods.
Jack Pine (PJ)	50	67.7	17.79 (0.39–28.97)	3.21 (−4.79–8.11)	Naturally occurring and planted jack pine stands at various densities.
White Pine (PW)	758	2781.6	26.58 (0.01–43.92)	2.38 (−4.928–12.55)	Stands dominated by white pine covering a range of plantations, managed and unmanaged natural stands in a mixture of red pine and an understory of other tree species, including poplar, spruce, and hardwoods.
Red Pine (PR)	170	322.8	23.52 (0.50–39.55)	2.45 (−4.98–11.30)	Natural and managed stands dominated by red pine in some cases with an understory of poplar and hardwoods.
Mixedwood conifer (MXC)	354	707.4	19.22 (0.75–35.97)	1.64 (−4.95–10.71)	Mixed species conifer stands with a range of species proportions dominated by black spruce, white spruce and balsam fir.
Mixedwood hardwood (MXH)	531	1342.7	22.95 (0.38–40.76)	1.43 (−4.985–11.33)	Hardwood mixed species stands with various species proportions of red maple, poplar and white spruce, with a lesser component of yellow birch, oak, balsam fir and white pine, among others.
Intolerant hardwood (INT)	368	871.3	22.95 (0.09–39.63)	2.28 (−4.92–12.79)	Natural stands dominated by poplar (large-tooth and trembling aspen leading) and often mixed with other hardwoods and conifers.
Tolerant hardwood (HD)	288	738.2	24.02 (1.89–42.86)	1.14 (−4.99–10.31)	Stands covering a range of structures and associated species (sugar maple, yellow birch, with a lesser component of red maple, beech, oak, hemlock, spruce and balsam fir).
Red Oak (OR)	405	1661.3	21.52 (1.02–41.66)	1.93 (−4.973–9.12)	Natural immature and mature oak dominant and oak-pine mixed stands, often with an understory of poplar and hardwoods.

forest characteristics across a regular tessellation of grid cells. Several ALS-based height percentiles are commonly used as a proxy measure of H_{TOP} in the literature, e.g., from the 95th to 100th percentile (Guerra-Hernández et al., 2021; Socha et al., 2020; Tompalski et al., 2022). However, the decision of the most suitable ALS metric to represent H_{TOP} is based on an empirical evaluation between the derived ALS percentiles and field-measured canopy height. In a previous analysis, we found the strongest correlation between the 99th percentile of first returns (zq99) and H_{TOP} calculated using repeated measurements of the TSP (Riofrío et al., 2022). Therefore, height (H_{TOP}) and total height increment (ΔH_{TOP}) were calculated at 25 m × 25 m cell size (625 m^2) to match the size of the TSP (14.1 m radius; 625 m^2) using the lidR package for R (Roussel et al., 2020). ΔH_{TOP} were calculated as the difference between consecutive ALS acquisitions (ALS_{2005} - ALS_{2012} and ALS_{2012} - ALS_{2018}) at the cell level, and the periodic annual height increments (PAI, m yr^{-1}) were calculated as the height increment divided by the time interval between ALS acquisitions, assuming constant growth within. Additionally, to avoid edge effects, we only included cells that were completely enclosed in the stand polygons after generating a buffer area of 25 m that accounted for stand borders, forest trails, public roads, and wetland areas from the forest inventory. Cells with a negative height >40% of the initial height were classified as disturbed (assumed due to silvicultural interventions) and were not considered in the analysis because they might lead to a negative height growth rate index estimation that might not be representative (Moan et al., 2023). In addition, we calculated the proportion of disturbed cells for every stand polygon in the forest inventory, and stands with more than 40% of cells classified as disturbed were also excluded from the analysis.

2.4. Height growth modeling approach

We used a dynamic top height model derived from the SDE approach that incorporates random elements into ordinary differential equations, representing the effects of a noisy environment on rates of change (García, 2019, 1983). The growth model for height (Eq. (1)) is the integral solution of the differential equation of the Bertalanffy-Richards growth rate model with a power transformation (García, 1983; Salas-Eljatib, 2020). Furthermore, Eq. (1) is a cumulative growth equation that has been applied successfully for modeling height growth for different species and environments (Hu and García, 2010; Orrego et al., 2021; Salas-Eljatib, 2021; Salas et al., 2008). Additional characteristics of Eq. (1) are that it allows for the prediction of height increments for different period lengths and for obtaining instantaneous growth estimates based on height as a state variable instead of age (Salas et al., 2008).

$$h = \alpha\left\{1 - \left[1 - \left(\frac{h_0}{\alpha}\right)^{\gamma} exp^{(-\beta(t-t_0))}\right]\right\}^{1/\gamma} \quad (1)$$

where h, t and h_0, t_0 are the height and year-date at the end and beginning of the period, respectively. The period length is obtained by $t - t_0$. The α, β and γ are the asymptote, rate of change, and shape-related parameters, respectively. As pointed out by Garcia (1983), when $t_0 = h_0 = 0$ in most forestry applications, the yield function Eq. (1) becomes the following growth function suitable for modelling height growth of even-aged forest populations:

$$h = \alpha\left[1 - exp^{-\beta(t)}\right]^{1/\gamma} \quad (2)$$

Based on function Eq. (1), Salas-Eljatib (2020) proposed a growth rate function independent of time that can be applied to in uneven-aged stands as an alternative to the traditional SI (height at a reference age) to quantify site quality. First, a growth rate function is obtained from the derivative for height of Eq. (2)

$$\frac{dh}{dt} = \frac{\alpha\beta}{\gamma}\left[1 - exp^{-\beta(t)}\right]^{\frac{1}{\gamma}-1}\left(exp^{-\beta t}\right) \quad (3)$$

To obtain a growth rate function depending on the state variable h, t in Eq. (3) is replaced by h raising both sides of Eq. 2 by γ, then solving for both exponential terms in Eq. (3), which gives

$$\frac{dh}{dt} = \left(\frac{\beta}{\gamma}\right) h\left[\left(\frac{\alpha}{h}\right)^{\gamma} - 1\right] \quad (4)$$

Eq. (4) express the rate of height change only as function of the value of the state variable h, not depending on time t. Based on Eq. (4), height growth–rate index (S) at a reference-height (h_r) function might be defined to build a system of height growth curves as indicator of site quality considering $h = h_r$ and $S = \frac{dh}{dt}$ in Eq. (4). Then solving and replacing for β in Eq. (4) yields the following expression:

$$\frac{dh}{dt} = \left(\frac{S}{h_r}\right) h\left[\left(\frac{\alpha}{h}\right)^{\gamma} - 1\right]\left[\left(\frac{\alpha}{h_r}\right)^{\gamma} - 1\right]^{-1} \quad (5)$$

where height growth–rate (dh/dt) depends on the height h, the growth rate site index S, the reference height h_r and the parameters α and γ from Eq. (1). The detailed steps of the mathematical derivation of Eq. (1) and Eq. (5) are available in the Appendix A and B in Salas-Eljatib (2020).

The growth rate model is both height-reference (h_r) and growth rate index (S) invariant in the same sense that a base-age invariant property is desirable for a traditional site index model (Skovsgaard and Vanclay, 2008). Eq. (5) does not depend on the choice of reference height or the growth rate index and different set values might be used (Salas-Eljatib, 2020). The reference height is arbitrary and user-defined value analogous to the reference age for height-age site index models. The selected reference height is a balance between the size at which the most dominant trees would have surpassed the initial period of intense competition following their establishment and a height that can be conveniently measured (Salas-Eljatib, 2020). The growth rate index define the site quality classes, for example, S=0.5 and $h_r = 15$ m refer to growth rate of 0.5 m yr^{-1} at the height of 15 m. Thus, age-independent top height (Eq. (1)) and site quality models (Eq. (5)) can be developed and applied to more complex, uneven-aged, and mixed-species forests, where age is not necessarily available from inventory and monitoring data.

2.5. Height growth model fitting from ALS data

ALS data has the potential to characterize the spatial variability in height increments across extensive areas and forest structures (Riofrío et al., 2022). H_{TOP} and ΔH_{TOP} derived from ALS zq99 metric in each 25 m grid cell along with forest type information assigned to each stand polygon were used to obtain height increments-height (ΔH_{TOP}-H_{TOP}) pairs for both periods (2005–2012 and 2012–2018). The aggregation of these pairs from different stands allows the reconstruction of the trajectory and variability of height growth rate for different stand development stages by forest type. Top height models were fit for each forest type (Table 1), as modeling height growth will most likely be species-dependent (Weiskittel et al., 2011).

The dynamic top height equation (Eq. (1)) was fit in a nonlinear mixed-effects model framework (NLME) to consider the temporally correlated and hierarchically nested structure of the data. Each cell has three observations of height over time (i.e., temporally correlation), and they are part of enclosed stand polygons (i.e., cells nested within stand polygons). The nested structure and correlation among repeated measures violate the basic assumption of independence in the data and may lead to biased estimates of the variance of the model parameters (Pinheiro and Bates, 2000). We tested different combinations of random effects to determine which parameters (α, β and γ) should include both fixed and random components. We consider the cells nested within stand polygons and growth period as random components. First, all fixed effect parameters were assumed to be random, with a general positive definite variance–covariance structure for the random effects. If this model failed to converge, then the number of random parameters was reduced to achieve convergence. The significance of the random effect was based on the likelihood ratio test ($p < 0.05$) between nested models. We defined the stochastic component of the model by including random effects on the α parameter as follows:

Table 3
Summary of airborne laser scanning (ALS) data acquisitions. LML: Linear-mode LiDAR and SPL: single photon LiDAR.

Data characteristics	ALS_{2005}	ALS_{2012}	ALS_{2018}
Acquisition month	September	August	July
Sensor	Leica ALS40	Riegl Q680i	Leica SPL100
Sensor type	LML	LML	SPL
Horizontal projection	UTM Zone 17N	UTM Zone 18N	UTM Zone 18N
Horizontal datum	NAD83 (CSRS)	NAD83 (CSRS)	NAD83 (CSRS)
Vertical datum	NAVD88	CGVD28	CGVD2013
Average point density (points m^{-2})	0.5	10	32
Average flying altitude (m a.g.l.)	2740	750	3760
Maximum pulse repetition frequency (kHz)	32	150	60
Scan angle (degrees)	±20	±20	±15
Laser wavelength (nm)	1064	1550	532

Table 2
Plot-level attributes of field sample plots. Top height increment values correspond to the period 2012–2018.

Forest type	n	Basal area (m^2 ha^{-1})	Quadratic mean diameter (cm)	Top height (m)	Total top height increment (m)
White Spruce (SW)	9	23.7 (12.3–38.2)	19.9 (14.3–28.1)	17.6 (9.83–29.8)	2.31 (0.510–4.18)
Jack Pine (PJ)	3	27.4 (22.7–31.7)	15.6 (14.4–17.2)	20.4 (19.7–20.8)	1.66 (0.927–2.04)
White Pine (PW)	54	28.0 (1.85–56.5)	29.2 (15.1–60.5)	29.0 (10.8–38.7)	2.02 (−5.8–11.7)
Red Pine (PR)	20	34.5 (12.6–78.1)	24.2 (11.3–44.8)	22.6 (6.53–36.4)	1.55 (−2.91–4.16)
Mixedwood conifer (MXC)	12	28.3 (1.96–60.4)	19.2 (10.2–40.7)	22.0 (9.43–38.2)	1.08 (−1.10–4.1)
Mixedwood hardwood (MXH)	23	22.8 (8.55–46.6)	19.5 (13.0–28.6)	24.4 (8.90–43)	0.499 (−4.3–3.27)
Intolerant hardwood (INT)	20	19.0 (0.272–39.7)	19.6 (11.1–68.6)	23.0 (9.1–35.7)	1.59 (−10.6–7)
Tolerant hardwood (HD)	23	31.4 (14.7–50.9)	27.6 (17.3–38.0)	27.3 (20.1–35.2)	1.52 (−3.5–8.1)
Red Oak (OR)	9	23.3 (13.2–28.7)	20.1 (12.2–24.8)	21.7 (14.8–31.6)	1.34 (−0.569–2.5)

$$H_{TOPijk} = (\alpha + a_{ij} + a_k)\left\{1 - \left[1 - \left(\frac{H_{TOP0ijk}}{\alpha + a_{ij} + a_k}\right)^{\gamma} exp^{\left(-\beta\left(t_{ijk} - t_{0ijk}\right)\right)}\right]\right\}^{1/\gamma} + \epsilon_{ijk} \quad (6)$$

where H_{TOPijk} is the H_{TOP} for the ith cell within the jth stand at the kth period and $H_{TOP0ijk}$ is the H_{TOP} of the same cell at the beginning of the period (t_0), period length $\Delta t = t_{ijk} - t_{0ijk}$. The α, β and γ are considered fixed parameters; a_{ij} is a random effect parameter specific to the ith cell within the jth stand, a_k is a random period parameter, specific to the observations taken during the kth period; ϵ_{ijk} is an error term that is assumed to be independent and normally distributed with a mean of zero and constant variance, $(a_{ij})\ N(0,\sigma_1^2)$, $(a_k)\ N(0,\sigma_2^2)$ and $\epsilon_{ijk}\ N(0,\sigma_{res}^2)$, respectively. Additionally, the continuous first-order autoregressive (CAR1) procedure was used to account for residual autocorrelation. We verified mixed-effects model assumptions graphically (i.e., quantile–quantile, residual and empirical autocorrelation plots). All models were fit using the *nlme* package for R (Pinheiro and Bates, 2000).

In this study, we fit two independent top height models (Eq. (6)) using the ΔH_{TOP}-H_{TOP} pairs under two modelling approaches. In the first model (P_1), we only used the data from the first period (2005–2012). In the second model ($P_{1,2}$), data from both periods (2005–2012 and 2012–2018) were used. For each model, we calculated conditional R^2 values, which account for the explanatory power of both fixed and random effects and marginal R^2 to describe the proportion of variance explained by the fixed factors alone, and the root mean square error (RMSE, corrected by the number of parameters in each model) computed using the marginalized predictions as a measure of goodness-of-fit of the models. Comparison of the estimates between models (P_1 and $P_{1,2}$) was based on the root mean square error (RMSE) (corrected by the number of parameters in each model) and graphical examination of the residuals. Additionally, applying the parameter estimates from Eq. (6) by forest type in Eq. (5), we compared the growth rate site index of both modelling approaches. For each forest type, we derived a system of height growth rate curves for five different height growth rate classes (S = 0.3, 0.5, 0.7 and 0.9 m yr^{-1}) at the reference H_{TOP} (h_r) of 15 m.

2.6. Validation of height growth models

Evaluating the quality of a model using only the goodness of fit statistic does not necessarily reflect the true quality of the prediction (Calama et al., 2003). Therefore, we assessed the predictive ability of both top height models (P_1 and $P_{1,2}$) using an independent data set to validate the predictions. The developed models were validated using the TSP data as an independent data source to quantify the accuracy and precision of the models. The developed top height models (P_1 and $P_{1,2}$) for each forest type were used to estimate H_{TOP} in 2018 using the TSP measurements of 2012. We used the bias and relative bias (bias%) as a measure of over- and under-estimation, and the RMSE and relative RMSE (RMSE%) as a measure of the accuracy of the estimates of the model compared with TSP measurements of 2018, which were computed as follows:

$$bias = \frac{\sum_{i=1}^{n}(y_i - \hat{y}_i)}{n} \quad (7)$$

$$bias\% = \frac{bias}{\bar{y}} \times 100 \quad (8)$$

$$RMSE = \sqrt{\frac{\sum_{i=1}^{n}(y_i - \hat{y}_i)^2}{n}} \quad (9)$$

$$RMSE\% = \frac{RMSE}{\bar{y}} \times 100 \quad (10)$$

where y_i, $\hat{y}_i$ and $\bar{y}$ are the observed, predicted and average values, respectively; n was the total number of observations. Each predicted height value $\hat{y}_i$ was estimated by setting a_{ij} and a_k set to zero according to Eq. (6); i.e., marginal predictions were based only on fixed effects from the final models and estimated values for the random components (EBLUP) are zeroes, thus the obtained marginal residuals are the difference between the observed height and the predicted height using the fixed effects marginal model (Calama and Montero, 2005).

2.7. Mapping height growth rate index of mixedwood forests

To produce a wall-to-wall map of height growth rate index for the PRF, we applied the best performing model between the two approaches (P_1 or $P_{1,2}$) for each forest type using the 25 × 25 m height increment data from the ALS acquisitions. Height growth rate index for each cell was calculated by solving Eq. (5) for S as follow:

$$S = \frac{dh}{dt}\frac{h_r}{h}\frac{\left[\left(\frac{\alpha}{h_r}\right)^{\gamma} - 1\right]}{\left[\left(\frac{\alpha}{h}\right)^{\gamma} - 1\right]} \quad (11)$$

where dh/dt is the height growth rate observed in the cell calculated as the height difference between consecutive ALS acquisitions divided by the time interval, h is the H_{TOP} at the beginning of the interval, h_r is the selected reference height (15 m), and α and γ are the parameters for each forest type from the selected model (P_1 or $P_{1,2}$) from Eq. (6). Forest type was determined using the forest inventory and assigned to each grid cell with the corresponding ΔH_{TOP}-H_{TOP} pairs.

3. Results

3.1. Age-independent height growth models and sensitivity to data inputs

The parameter estimates for both P_1 and $P_{1,2}$ top height models (Eq. (6) and the corresponding RMSE values are shown in Table 4. For all forest types, the resulting parameter estimates were significant (p-value < 0.05) and similar between both P_1 and $P_{1,2}$ models. The RMSE indicated that the $P_{1,2}$ model generally provided the lower RMSE value and greater marginal and conditional R^2 for most forest types, except for the PJ forest type. Inspection of standardized residuals showed no concerns for the model assumptions (Supplementary information, Fig. S1) and the AIC of the $P_{1,2}$ models notably improved with the inclusion of the autocorrelation function in the model structure (Supplementary information, Fig. S2). Moreover, the variance of the random effects between polygons (σ_1^2) were greater than between periods (σ_2^2) when both random parameters were considered in the model. For 3 out of 9 forest types (PW, MXC and HD), the random effects at the period level did not improve the fit statistics and were not included in the $P_{1,2}$ final model. Only for PJ did we find that the inclusion of random effects at the polygon level did not improve the model in terms of AIC and only the period level was considered.

In order to illustrate the relationship between ΔH_{TOP} and H_{TOP} for different productivity levels among sites, we used Eq. (5) with the coefficients estimated from both modelling approaches (Table 4) by forest type. Similar to Salas-Eljatib (2020), for each forest type, we derived a system of height growth curves for four different growth rate index classes (0.3, 0.5, 0.7 and 0.9 m yr^{-1}) at the reference height of 15 m (Fig. 2). The height growth trajectories represent an age-independent height growth rate index, where the height growth levels only depend on the state variable height and not on age (Salas-Eljatib, 2020). PJ, MXC, MXH and OR forest types showed similar curve systems regardless of the data set used to fit the models (P_1 or $P_{1,2}$). Differences between models were observed for some forest types. For SW, PW, PR and HD, the major difference was noted at the initial development stages in the better sites. However, both models converged to a similar asymptote and decreasing rate. The greatest difference between models was found for INT stands, while the asymptote for the $P_{1,2}$ model was 4 m greater than

in the P_1 model, the rate parameter notably lower for the $P_{1,2}$ model.

3.2. Validation of height growth models

The accuracy of the fitted models to predict the H_{TOP} of the TSP is presented in Fig. 3 and Fig. 4. Overall, we found good agreement between predicted and observed values for all forest types. Only for PW (p-value < 0.05), the results of the paired *t*-test indicated that the null hypothesis that the difference between observed and predicted height values was different from 0. We also observed similar H_{TOP} predictions between both P_1 and $P_{1,2}$ models in terms of bias, bias%, RSME and RMSE%, with no systematic errors visible on the predicted versus observed values (Fig. 5). Except for SW and MXC forest types, the H_{TOP} predictions using the P_1 model were slightly improved (<0.14 RSME%) relative to the estimates using the $P_{1,2}$ model in terms of RMSE and RMSE%. Moreover, some variations in the magnitude of the accuracy and bias were observed among forest types (Table 5). PW, INT and HD showed the lowest accuracy of predicted H_{TOP} values, with RMSE% greater than 10%. For PW and HD, the predictions tend to overestimate the H_{TOP} in plots with heights greater than 35 m. Due to the low number of TSP plots (n = 3) and the restricted range of H_{TOP} values (19.7–20.8 m) (Table 2), the validation for PJ stands was considered not representative and was not reported.

3.3. Mapping height growth rate index of mixedwood forest

Models with the lowest RMSE for each forest type (Table 4) were used to map the height growth rate index at the reference height of 15 m (Fig. 2). The spatially explicit growth rate index map represents a site quality indicator for mixedwood forest in the PRF with a spatial resolution of 25 m (Fig. 6). The distribution of the growth rate index estimations was different among forests type, distinguishing two main groups (Fig. 7). MXC, MHC, HD and OR showed a right-skewed distribution with and median growth rate index of around 0.25 m yr^{-1} and lower site quality values. While SW, PJ, PW, PR and INT showed a more symmetrical distribution with a median growth rate index value between 0.36–0.43 and greater frequency of cells with site quality values above 0.5 m yr^{-1}.

4. Discussion

In this research, we developed age-independent top height growth models for different temperate mixedwood forests in the Great Lakes–St. Lawrence region, Ontario, Canada. Our approach demonstrates the feasibility of parametrizing age-independent top height growth models using multi-temporal ALS data. The capacity of repeated ALS acquisitions or image-based point clouds to reconstruct height growth trajectories and modelling site index has been explored previously (Noordermeer et al., 2020; Socha et al., 2017; Tompalski et al., 2015). However, our approach is novel as it can be applied to map spatially explicit top height projections and growth rate index as a proxy of site quality levels for more complex forest structures, where applying the traditional site index (i.e., based on the height-age relationship) has important limitations.

4.1. Age-independent height growth models and sensitivity to modelling approaches

Bi-temporal ALS and age-independent modelling strategies based on GADA functions have shown satisfactory results compared to age-dependent models (Guerra-Hernández et al., 2021; Solberg et al., 2019). However, this approach has only been applied to even-aged stands. The SDE, used in this research, and GADA are the two main approaches used to model top height and site index in forestry in the past decades (Burkhart and Tomé, 2012; Weiskittel et al., 2011). Both approaches have produced suitable H_{TOP} models and can even lead to similar functional forms, for instance, comparing the general function by Rennolls (1995) and the model CR1 by Krumland and Eng (2005). However, the most optimal statistical method for modeling H_{TOP} growth is still debated in the literature (García, 2011; Manso et al., 2021; Nigh and Aravanopoulos, 2015; Orrego et al., 2021).

We observed different height growth patterns depending on forest types. In a preliminary analysis, we could not find convergence for a general top height model including all forest types (i.e., a species-independent model), and the simple inclusion of forest type as a random effect improved the base model. Height growth patterns in even-aged stands are recognized to be species-specific (Skovsgaard and Vanclay, 2008) because tree species are adapted to different ecological niches and react differently to stand conditions such as competition or structure, and environmental factors such as climate conditions or soil attributes. However, for uneven-aged or irregular stands, height growth trajectories are expected to follow a different growth pattern than even-aged stands due to different size-diameter and size-height distributions as a result of suppression growth periods that reduced height increment due to overstory competition (Pretzsch, 2009; Weiskittel et al., 2011). Nevertheless, an interesting approach by Hennigar et al. (2017) based on biomass increment proposed a unified site productivity model applicable for multi-cohort and mixed-species stands over large spatial extent by combining climate, soils and topographic metrics with stand structure and species composition.

We evaluated the sensitivity of the models to different modelling approaches. Although we observed differences in the growth rate and height trajectories for some forest types depending on the period used to fit the models (Fig. 2), the validation analysis showed very similar predictive capacity between the P_1 and $P_{1,2}$ models when they were used to estimate H_{TOP} of the TSP data. However, we acknowledge the uneven distribution of TSP among forest types and along the range of H_{TOP} classes, especially underrepresenting stands at initial development stages (i.e., $H_{TOP} < 10$ m). This requires special attention because there is generally greater uncertainty in the height growth estimates observed for young stands (Weiskittel et al., 2011). In agreement with our results, Guerra-Hernández et al. (2021) tested different GADA model forms and underestimated height growth for young stands. Tymińska-Czabańska et al. (2021) likewise reported underestimating height growth in young stands when using different models for different periods using repeated ALS data.

Considering the hierarchical structure of the data in the NLME approach increased the proportion of variation in height accounted by the models. The variation of the asymptote parameter by including the polygon level effects appeared to account for the variation between stands characteristics. The combination of a regular structure of jack pine plantations and the lower number of available stands compared to other forest types in PRF (Table 1) support the fact that the polygon random effect was not included in the model for jack pine. Species diversity and long-term silviculture history characterize the structural complexity of stands in PRF (White et al., 2019). Structure, species composition, and management legacy effects strongly determine the growth trajectories, especially for more complex stands (Pretzsch, 2020). Including period level in the random structure of the models for most forest types has important implications because height increments for the same period in different stands are not independent because they are affected by similar weather conditions (García, 1983). In a previous analysis (Riofrío et al., 2022), we observed variability in the PAI values among different periods using the same ALS dataset. The fluctuations in the PAI values reflect that other factors, such as climate variability among growth periods or intrinsic forest growth dynamics, affect height growth.

Height growth and site index models calibrated using repeated ALS data have shown very similar growth trajectories compared to models based on stem analysis data (Socha et al., 2017; Tymińska-Czabańska et al., 2021). Moreover, (Socha et al., 2020) found that the grid cell size (10 × 10, 30 × 30 and 50 × 50 m) used to calculate the ALS metric did

Table 4
Estimated coefficients (and their standard errors) for the fitted the top height models by forest type Eq. (6), as well as variance components of the random effects (σ_1^2 and σ_2^2) and parameters for the autocorrelation structure (ρ). RMSE – root mean square error. For all forest types, the resulting parameter estimates were significant (p-value < 0.05).

Forest type	Model	α	β	γ	σ_1^2(polygon)	σ_2^2(period)	σ_{error}^2	ρ	RMSE	R^2 marginal	R^2 conditional
SW	P_1	30.4399	−0.0327	0.9096	16.2522		0.5396		0.705	0.9546	0.9791
		(0.8434)	(0.0026)	(0.0766)							
	$P_{1,2}$	31.5339	−0.0289	0.9810	10.1117	4.0948	0.4122	0.1477	0.614	0.9667	0.9836
		(0.6328)	(0.0016)	(0.0557)							
PJ	P_1	28.5063	−0.0365	0.8124	4.2171		0.4203		0.611	0.9436	0.9555
		(0.7583)	(0.0028)	(0.0865)							
	$P_{1,2}$	27.6120	−0.0337	0.8118		1.5765	0.3237	0.3375	0.779	0.9555	0.9618
		(0.9522)	(0.0017)	(0.0583)							
PW	P_1	43.7382	−0.0132	0.8483	28.0771		0.9374		0.960	0.9341	0.9436
		(0.4874)	(0.0005)	(0.0453)							
	$P_{1,2}$	44.1374	−0.0111	0.9344	26.6507		0.7946	0.0390	0.887	0.9470	0.9534
		(0.4132)	(0.0003)	(0.0389)							
PR	P_1	33.9329	−0.0239	0.9045	23.4506		0.9283		0.945	0.9630	0.9731
		(0.6691)	(0.0015)	(0.0462)							
	$P_{1,2}$	35.0058	−0.0198	0.9507	15.8465	7.0600	0.4235	0.1095	0.636	0.9787	0.9870
		(0.47103)	(0.0005)	(0.0313)							
MXC	P_1	31.5449	−0.0179	0.9518	53.5866		1.2959		1.12	0.9267	0.9486
		(0.5550)	(0.0005)	(0.0816)							
	$P_{1,2}$	32.3103	−0.0144	0.9682	82.7256		0.7505	0.2228	0.852	0.9499	0.9699
		(0.6081)	(0.0003)	(0.1946)							
MXH	P_1	36.9114	−0.0127	0.9203	28.2250		0.6463		0.803	0.9651	0.9713
		(0.4216)	(0.003)	(0.0504)							
	$P_{1,2}$	37.9677	−0.0110	0.9394	34.6246	10.7422	0.5835	0.0778	0.755	0.9671	0.9740
		(0.3956)	(0.0002)	(0.0410)							
INT	P_1	32.5363	−0.0254	0.8589	17.3676		1.1448		1.05	0.9358	0.9535
		(0.3123)	(0.0005)	(0.0495)							
	$P_{1,2}$	36.6768	−0.0146	0.8736	33.1129	1.1609	0.0961		0.706	0.9692	0.9778
		(0.4233)	(0.0002)	(0.0426)							
HD	P_1	34.8144	−0.0111	0.7811	35.2332		1.1677		1.070	0.9253	0.9334
		(0.6133)	(0.0004)	(0.1268)							
	$P_{1,2}$	34.1655	−0.0106	0.8563	36.0467		0.9228	0.1464	0.952	0.9397	0.9470
		(0.5178)	(0.0003)	(0.1145)							
OR	P_1	33.4578	−0.0161	0.7210	25.7669		1.0268		1.010	0.9208	0.9335
		(0.4094)	(0.0006)	(0.0717)							
	$P_{1,2}$	33.1844	−0.0149	0.7080	18.4942	9.0804	0.7509	0.0907	0.860	0.9277	0.9401
		(0.3426)	(0.0004)	(0.0569)							

not affect the height growth trajectories. Using the ABA approach to quantify height growth is more common than the individual tree detection (ITD) approach because of the greater likelihood of missing individual tree tops when using ALS acquisitions with different point densities (Zhao et al., 2018). Also, the tree detection and crown delineation algorithms cannot be reliably applied when point density is low (Tompalski et al., 2021). Moreover, differences in point density among acquisitions likely have very little influence on ABA-derived height percentiles metrics because the spatial distribution of the point cloud is similar, even if the point density varies markedly (Zhao et al., 2018).

Additionally, the accuracy of the digital elevation models used to normalize the point clouds is known to vary with topographic complexity, the overlying vegetation and the characteristics of the ALS acquisitions (White et al., 2021b). Repeated ALS data are often acquired with different levels of horizontal and vertical accuracy and may use different horizontal or vertical datums. Harmonization of multi-temporal ALS data sets (e.g., projection and/or datum transformation) is required to ensure that changes detected in 3D point clouds represent real changes in the target of interest and do not result from differences in the data itself (Riofrío et al., 2022). Neglecting the assessment of the vertical alignment among multi-temporal ALS may bias the derived height increments, especially where there are short-time intervals between ALS acquisitions (Riofrío et al., 2022). Therefore, biasing the estimated growth trajectories for mature and old stands when the growth rate decreases close to 0.

4.2. Validation of height-growth models

We assessed our developed top height models using increments derived from repeated field measurements (TSPs). Results from the TSP data indicated that model performance varied by forest type (Fig. 3 and Fig. 4) and height class (Fig. 5). Inclusion of height increment from two periods generally improved model performance relative to models developed using height increment from a single period; however, the degree of improvement varied by forest type and was relatively minor. The majority of studies in the literature that have reported on using ALS (or digital aerial photogrammetry – DAP) data to assess growth have considered only a single period (i.e., using two ALS acquisitions; see Table 1 in Tompalski et al. (2021)). Hopkinson et al. (2008) analyzed four different ALS acquisitions and three time periods (2000–2002, 2002–2004, 2004–2005), and reported that height growth—as measured for each period—was statistically significant, relatively consistent over time, and similar to the observed field growth estimate derived for 2000–2005. However, Hopkinson et al. (2008) studied plantation forests and growth periods considered spanned a narrower temporal window than we considered herein (2005–2018). Skowronski et al. (2014) likewise concluded on the consistency of ALS biomass change estimation for three different periods (2004–2007, 2007–2009, 2004–2009) and reporting that the longer period (2004–2009) resulted in the greatest increase in efficiency for the model estimation. Zhao et al. (2018) estimate biomass change using four ALS acquisitions (2002, 2006, 2008 and 2012) and two repeated field inventories (2002 and 2006) demonstrating the transferability of the calibrated model using the 2002–2006 period to estimate biomass change and canopy dynamics

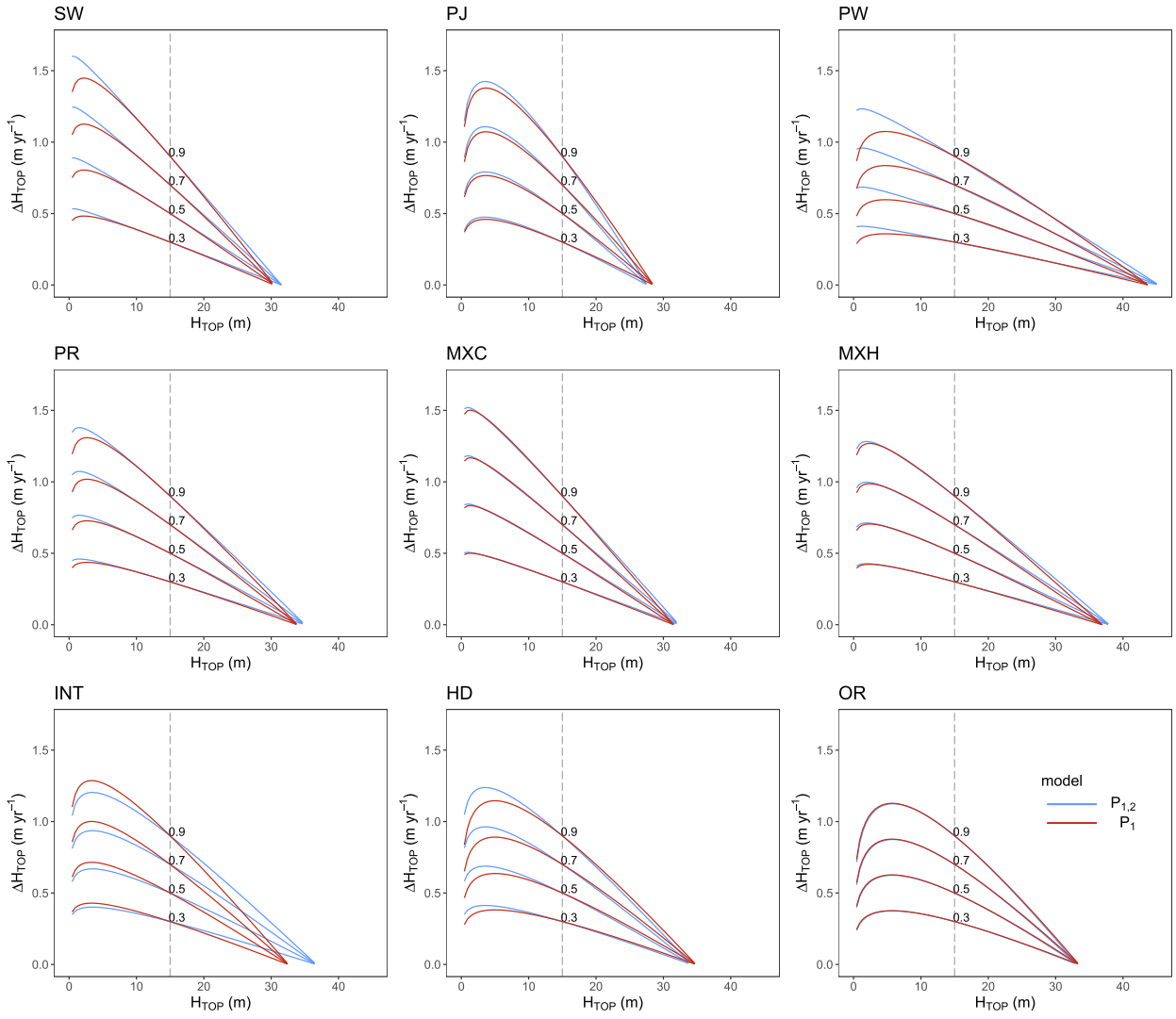

Fig. 2. Height growth rate versus the height for different modelling approaches, P_1 (red lines) and $P_{1,2}$ model (blue lines). Curve systems are age-independent growth rate indices for five different site quality classes (0.3, 0.5, 0.7 and 0.9) at the reference height of 15 m (dashed line). (For interpretation of the references to colour in this figure legend, the reader is referred to the web version of this article.)

in the subsequent periods.

4.3. Age-independent height and height growth-rate models in forest management and planning

Due to the long-term silviculture history that characterizes PRF and the variety of partial harvesting regimes, uneven-aged or mixed-species stands are not indicative of the actual productivity of the different tree species. Therefore, developing more flexible methods to estimate height growth and site quality adapted to complex forest structures is required. Repeated ALS data provide the opportunity to characterize the current state and changes in forest attributes at a fine spatial scale over large areas and time (Coops et al., 2021; White et al., 2016). As we demonstrated herein, height growth trajectories extracted from multi-temporal ALS enable the development of a site quality indicator for structurally uneven-aged and mixed-species forests, which often lack representation in forest inventories and G&Y models. Moreover, ALS can capture a broad range of forest conditions and represent contemporary height growth measures under changing climatic conditions. The approach presented herein provides wall-to-wall measures of site quality at a higher spatial resolution over a full forest management unit that can be readily used in tree and stand growth and yield modeling.

The capacity to generate this spatially explicit output is one of the strengths of using ALS data. Previous studies have generated and mapped SI by combining known age-height curves and time series of canopy height models (Véga and St-Onge, 2009), ALS data in combination with registered stand age (Socha et al., 2017), or age derived from Landsat time series (Tompalski et al., 2015). However, such methods depend on the availability of stand age data and the height-age relationship, which might be meaningless in uneven age and complex stands. Castaño-Santamaría et al. (2023) developed a site form index (dominant height of a stand at a reference dominant diameter) for predicting and mapping site quality. However, the application of the method may be problematic because of the sensitivity of diameter growth to stand density, which alters the dominant height–dominant diameter relationship (Wang, 1998; Weiskittel et al., 2011). Moreover, there is greater uncertainty in generating reliable dominant diameter estimates from ALS data, which could bias the site quality values.

As the height growth rate index depends on the height increment for a given period, caution is advised in applying the index where there are negative ΔH_{TOP} values, which can result in non-representative negative growth rate index estimations. Such negative ΔH_{TOP} values may be associated with disturbance and mortality in the stand. It is also important to note that for a given grid cell with an initial or final H_{TOP}

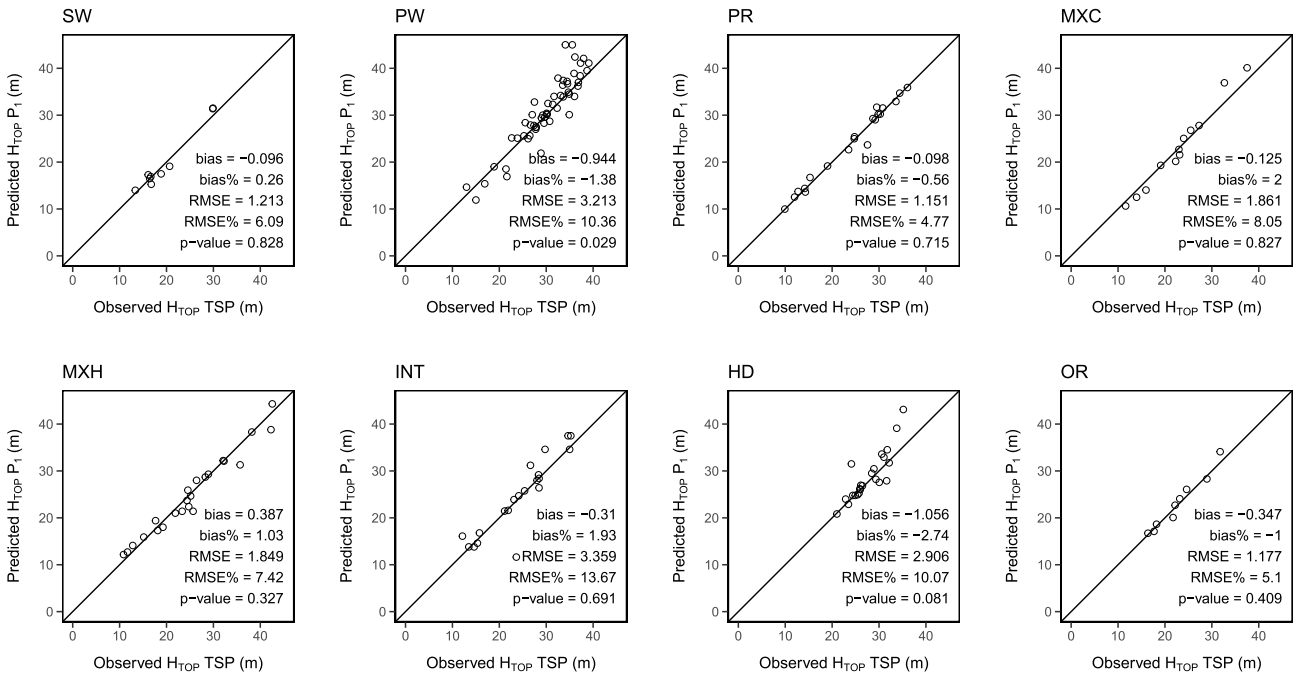

Fig. 3. Predicted H_{TOP} from the models P_1 compared with observed H_{TOP} from TSP measurements. See Table 1 for forest types.

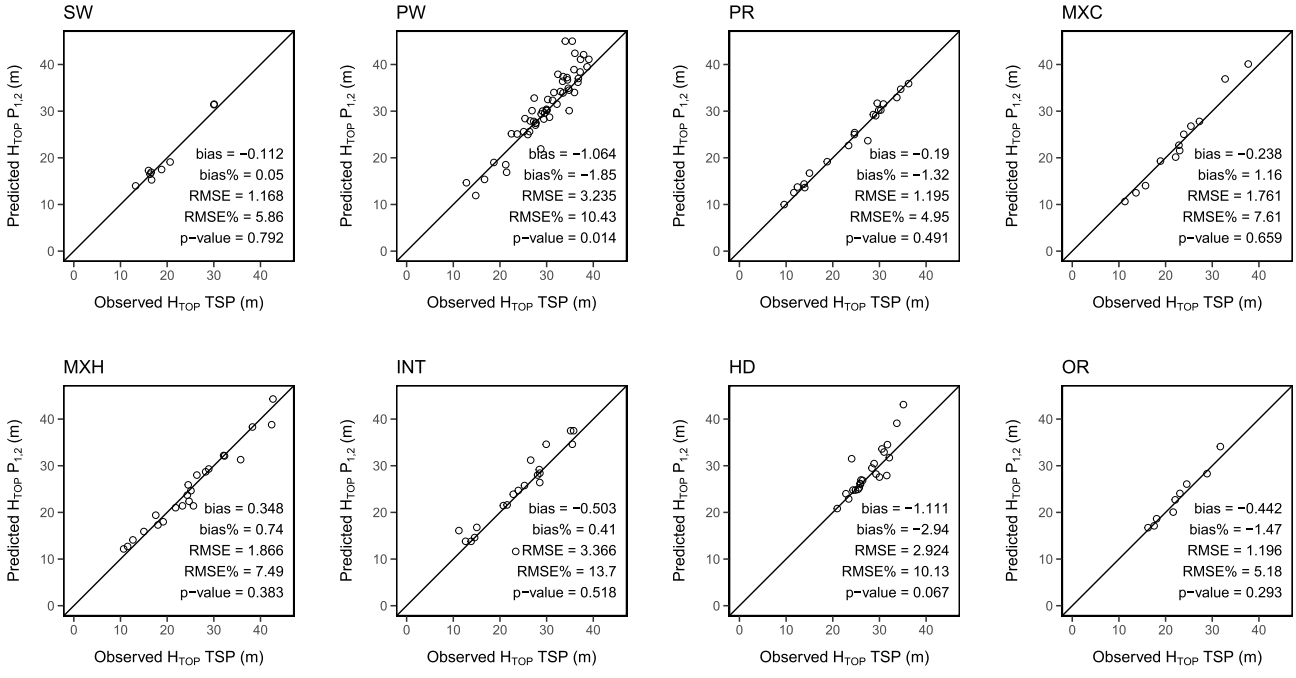

Fig. 4. Predicted H_{TOP} from the models $P_{1,2}$ compared with observed H_{TOP} from TSP measurements. See Table 1 for forest types.

greater than the asymptote values of the model, the growth rate index estimation may fall outside the range of expected values. Therefore, in order to avoid extrapolation errors, we assumed that those grid cells corresponded to the highest growth rate index class within their given forest type.

Although a full demonstration of the link between the growth rate index presented herein and productivity (in terms of volume or timber production, $m^3 \cdot ha^{-1} \cdot year^{-1}$) remains to be investigated it is anticipated a relationship should exist; for instance, the extended Eichhorn's rule postulates that any two stands with identical height growth and identical initial height will have identical volume growth, irrespective of any differences in age (Skovsgaard and Vanclay, 2008). This implies that stand volume growth can be estimated from height growth by using a general model or a reference stand with known volume growth, then defining the yield level. However, yield levels (volume growth estimates) might be affected by climate, soil, provenance, establishment method, stand treatment or other factors (Assmann, 1970). Increment-based indices, i.e., dominant height or basal area increment, have been conducted at the stand-level as an suitable empirical SI method for multi-aged stands (Berrill and O'Hara, 2014). However, this approach depends on accurate remeasurement of height, which is one of the strengths of derived ALS height increments.

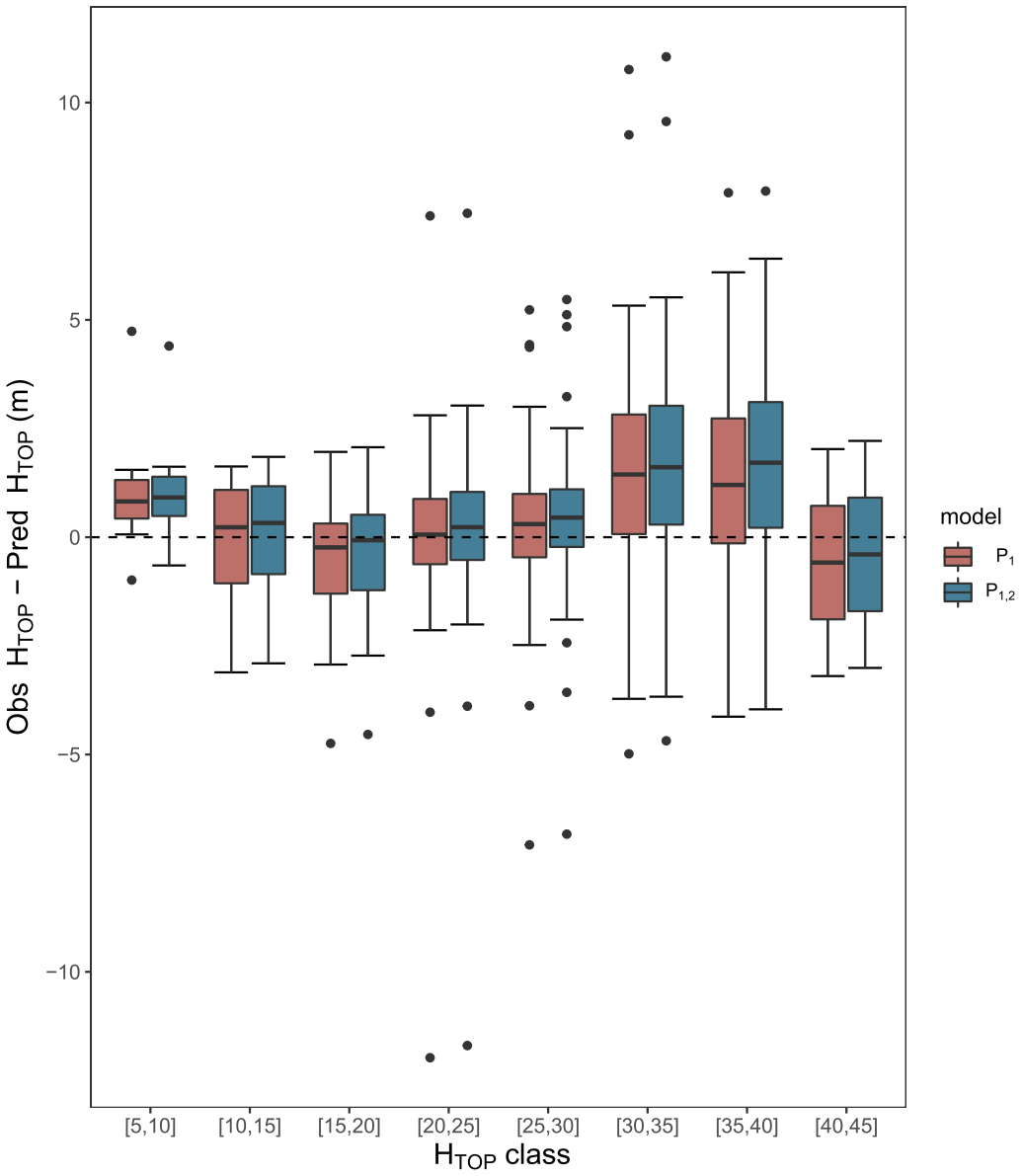

Fig. 5. Difference between observed H_{TOP} from TSP measurements and predicted H_{TOP} values by modeling approach (P_1, $P_{1,2}$).

Table 5
Validation statistics between predicted (from ALS) and observed (from TSP) Top height values using fitted models.

Forest type	Model	n plots	Bias	Bias%	RMSE	RMSE%
SW	P_1	9	0.096	0.26	1.213	6.09
	$P_{1,2}$		−0.112	0.05	1.168	5.86
PW	P_1	57	−0.944	−1.38	3.213	10.36
	$P_{1,2}$		−1.064	−1.85	3.235	10.43
PR	P_1	20	−0.098	−0.56	1.151	4.77
	$P_{1,2}$		−0.190	−1.32	1.195	4.91
MXC	P_1	12	0.125	2.00	1.861	8.05
	$P_{1,2}$		0.238	1.16	1.761	7.61
MXH	P_1	23	0.387	1.03	1.849	7.42
	$P_{1,2}$		0.348	0.74	1.866	7.49
INT	P_1	20	0.310	1.93	3.359	13.67
	$P_{1,2}$		0.503	0.41	3.366	13.70
HD	P_1	23	−1.056	−2.74	2.906	10.07
	$P_{1,2}$		−1.111	−2.94	2.924	10.13
OR	P_1	9	−0.347	−1.00	1.177	5.10
	$P_{1,2}$		0.442	−1.47	1.196	5.18

Overall in mixedwood (MXC, MHC), intolerant hardwood (HD), and oak-dominated stands (OR), median values of the height growth rate index were lower and had a right-skewed distribution compared to the symmetrical distributions of growth rate index values for growth rate white spruce (SW), pine (PJ, PW, PR), and intolerant hardwood (INT) dominated stands. Wall-to-wall height growth rate index information allows for spatially explicit monitoring of site quality within a stand, enhancing the usefulness of the data for forest management planning. For example, white spruce and jack pine plantations (SW and PJ) showed a clear peak distribution around median growth rate values with a greater frequency of grid cells with site quality above 0.5, also reflecting stands with more intense management activities that should optimize the carrying capacity and increase the productivity (Oliver and Larson, 1996). In contrast, PW and PR showed a symmetrical but flatter distribution of growth rate values, forest type that group managed and unmanaged natural stands (Table 1). The right-skewed distribution for MXC, MHC, HD and OR forest types illustrated the more complex structures with greater variations in stand density, species composition, vertical structure and competition (Berrill and O'Hara, 2014; del Río et al., 2016). Furthermore, a continuous and high spatial resolution site

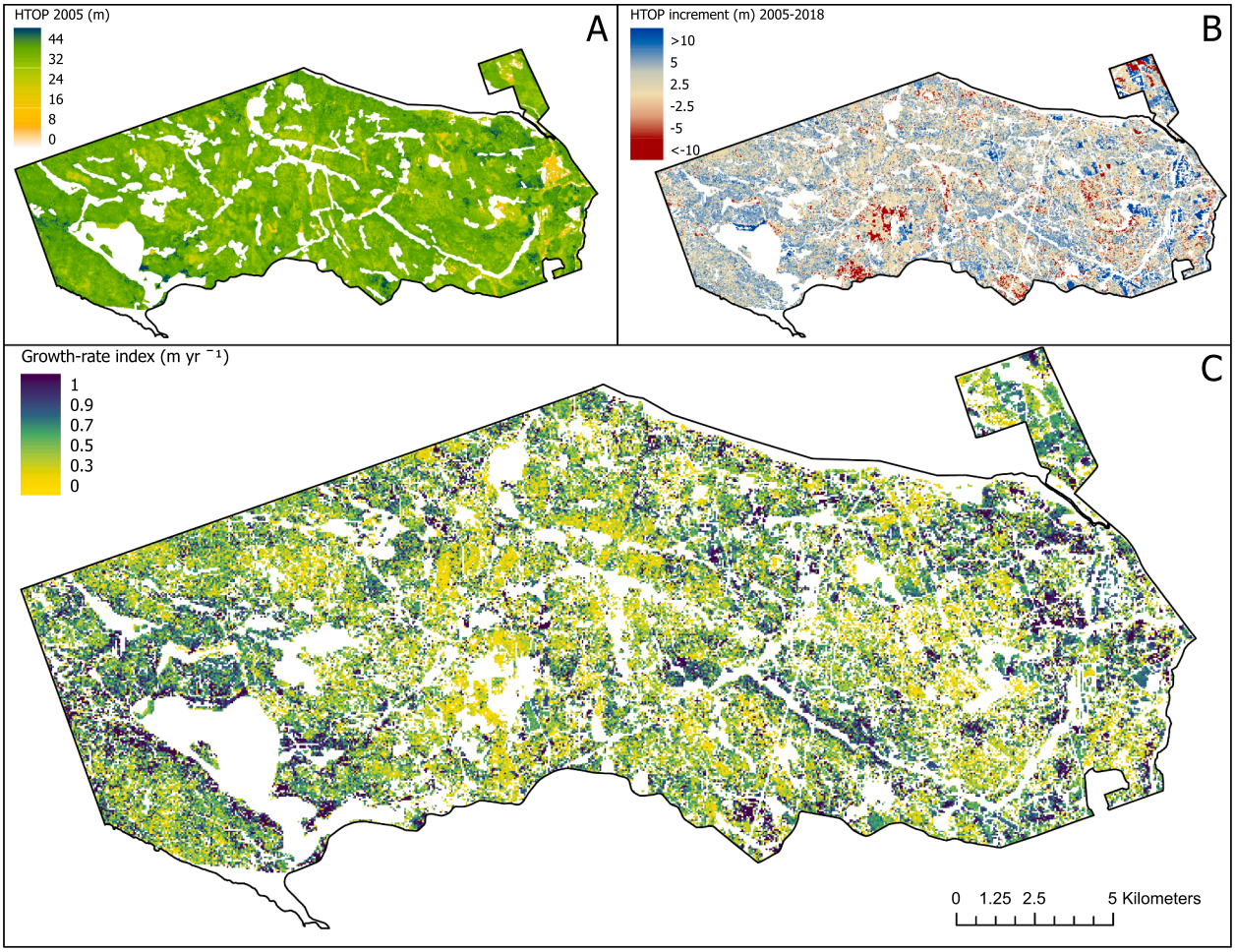

Fig. 6. (A) H_{TOP} from the ALS_{2005} acquisition, (B) H_{TOP} increment between ALS_{2005} and ALS_{2018} acquisitions and (C) growth rate index at 25 m spatial resolution. White areas represent grid cells excluded from mapping: stand borders, forest trails, public roads, wetlands and disturbed areas.

quality map opens the possibility to analyze the spatial correlation of productivity with other variables like soil and climate attributes.

In this study, we used data from a forest inventory to assign the forest type to each grid cell based on the dominant species determined through manual interpretation of digital aerial imagery at the stand level. However, we acknowledge the uncertainty in photo-interpreted species compositions, and if a different species is dominant in a given cell, these misclassifications can add noise to the fitted model and result in incorrect estimates of site quality. An alternative approach to classifying dominant tree species in individual grid cells might involve integrating data from both ALS and Sentinel-2 imagery (e.g., Queinnec et al., 2022), which could provide area-based predictions of species groups at a more detailed spatial resolution than the stand-level estimates from the photo-interpreted data.

Our approach offers several advantages towards improving the available forest management decision tools and integrating different remote sensing sources to enable reliable estimation of height growth and site quality. The main advantage of the approach presented is being independent of age data, as noted previously in the context of the applicability of the models to more complex forest structures. Age is time-consuming and relatively difficult to measure accurately. Moreover, the fact that age is not available at the same spatial resolution as the ALS data constrains the application of spatially explicit models. Furthermore, developing top height and site productivity models based on ALS metrics (i.e., zq99) instead of ALS-derived forest attributes (i.e., top height estimated from linear regression using ground plot measures and ALS metrics) minimizes and simplifies the uncertainty estimation associated with the final predictions (Saarela et al., 2020). Thus, G&Y models might take full advantage of the strength of spatially explicit forest attributes generated from the more frequent ALS data. Our results demonstrated that in these forest types, models developed using bi-temporal ALS data for a single period had similar performance to models developed using ALS data for two periods (developed using multi-temporal ALS). As bi-temporal ALS data are currently more widely available than multi-temporal ALS data, this result suggests that the approach developed herein is robuts in areas where only bi-temporal ALS data are available. However, in some areas, even bi-temporal ALS data are not yet widely available either. Alternatively, the combination of ALS data and digital aerial photogrammetry also has potential for providing information on canopy heights and height changes from different time periods (Stepper et al., 2014; Tompalski et al., 2019). Furthermore, such a multi-sensor approach may allow for evaluating the shifts in site productivity and even long trends in forest dynamics affected by environmental factors that include biotic, edaphic, and climatic conditions (Salas-Eljatib, 2021; Tymińska-Czabańska et al., 2021). Additionally, tree diameter growth models might also be developed relying completely on a single acquisition of ALS metrics (Maltamo et al., 2022). Finally, the potential of new algorithms to generate height growth trajectories from a single acquisition of high-density ALS data (Puliti et al., 2022) could also be used for forecasting height growth and estimating site quality using the approach presented herein.

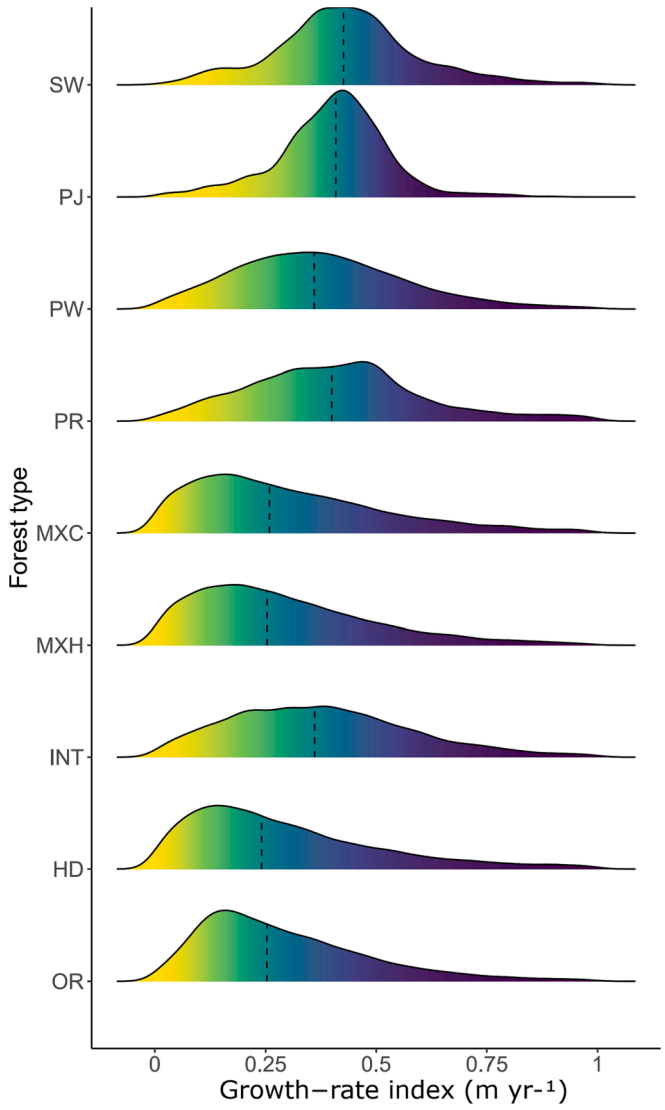

Fig. 7. Distribution of growth rate index estimations by forest type in the PRF. Dashed lines represent the 0.5 quantile (median value) of the distribution.

5. Conclusion

Site index remains the primary means of estimating and evaluating site productivity, but the application of site index for more uneven-aged and mixed-species stands has several limitations. Hence, developing more flexible methods for characterizing productivity adapted to complex forest structures is required. The approach presented herein takes advantage of a key strength of ALS data—the accurate capture of canopy heights across large spatial extents and with fine spatial detail—while also minimizing dependence on age, an attribute that is very difficult to measure accurately and that is often estimated more broadly at the stand level. Using independent data for assessment, predicted heights had good agreement with observed values for all forest types. Therefore, key value added by this research is the development of an age-independent height growth rate index and associated height estimates for application to heterogeneous, temperate mixedwood forests. Integrating multi-temporal ALS data and an age-independent approach allows for the mapping of height increments over large areas at a finer spatial resolution than is commonly possible with conventional forest inventory data and stand-level, age-dependent, models. Moreover, the growth rate index provides a continuous measure of site quality at a high spatial resolution that can be readily used in forest growth and yield modeling. The approach developed and demonstrated here can be adapted to multi-sensor data sources (ALS and DAP) that would increase the data available to support spatially explicit characterizations of height and height growth over large spatial extents.

CRediT authorship contribution statement

José Riofrío: Conceptualization, Data curation, Formal analysis, Investigation, Methodology, Writing – original draft. **Joanne C. White:** Conceptualization, Formal analysis, Funding acquisition, Methodology, Resources, Supervision, Writing – review & editing. **Piotr Tompalski:** Conceptualization, Methodology, Writing – review & editing. **Nicholas C. Coops:** Conceptualization, Funding acquisition, Project administration, Resources, Supervision, Writing – review & editing. **Michael A. Wulder:** Conceptualization, Funding acquisition, Project administration, Resources, Writing – review & editing.

Declaration of Competing Interest

The authors declare that they have no known competing financial interests or personal relationships that could have appeared to influence the work reported in this paper.

Data availability

The link to access the data was provided in the acknowledgments section

Acknowledgments

This work was supported with funds from the Canadian Wood Fibre Centre (CWFC) of the Canadian Forest Service. Murray Woods and Dr. Margaret Penner are thanked for compiling and sharing the field data for 2012 and 2018. Field data were collected through funds provided by the CWFC and the Ontario Forestry Future's Trust. ALS data were provided by Ontario Ministry of Northern Development, Mines, Natural Resources and Forestry and the CWFC. Thanks to Christian Salas-Eljatib (Universidad Mayor, Chile) for his valuable comments and modeling recommendations in a previous version of this work. We thank the editor and two anonymous reviewers for their constructive comments and suggestions for improvement. Both the ALS and field measurements data used in our analysis are openly available on the Petawawa Research Forest remote sensing supersite: https://opendata.nfis.org/mapserver/PRF.html.

Appendix A. Supplementary data

Supplementary data to this article can be found online at https://doi.org/10.1016/j.foreco.2023.121137.

References

Andersen, H.E., Reutebuch, S.E., McGaughey, R.J., 2006. A rigorous assessment of tree height measurements obtained using airborne lidar and conventional field methods. Can. J. Remote Sens. 32, 355–366. https://doi.org/10.5589/m06-030.

Anyomi, K.A., Raulier, F., Bergeron, Y., Mailly, D., Girardin, M.P., 2014. Spatial and temporal heterogeneity of forest site productivity drivers: a case study within the eastern boreal forests of Canada. Landsc. Ecol. 29, 905–918. https://doi.org/10.1007/s10980-014-0026-y.

Assmann, E., 1970. The Principles of Forest Yield Study. Studies in the Organic Production, Structure, Increment and Yield Of Forest Stands. Pergamon Press, New York, NY.

Berrill, J.P., O'Hara, K.L., 2014. Estimating site productivity in irregular stand structures by indexing the basal area or volume increment of the dominant species. Can. J. For. Res. 44, 92–100. https://doi.org/10.1139/cjfr-2013-0230.

Bravo, F., Fabrika, M., Ammer, C., Barreiro, S., Bielak, K., Coll, L., Fonseca, T., Kangur, A., Löf, M., Merganičová, K., Pach, M., Pretzsch, H., Stojanović, D., Schuler, L., Peric, S., Rötzer, T., Del Río, M., Dodan, M., Bravo-Oviedo, A., 2019. Modelling approaches for mixed forests dynamics prognosis. Research gaps and opportunities. For. Syst. 28, 1–18. https://doi.org/10.5424/fs/2019281-14342.

Burkhart, H.E., Tomé, M. (Eds.), 2012. Modeling Forest Trees and Stands. Springer Netherlands, Dordrecht.
Calama, R., Cañadas, N., Montero, G., 2003. Inter-regional variability in site index models for even-aged stands of. Ann. For. Sci. 60, 259–269. https://doi.org/10.1051/forest.
Calama, R., Montero, G., 2005. Multilevel linear mixed model for tree diameter increment in stone pine (Pinus pinea): A calibrating approach. Silva Fenn. 39, 37–54.
Carmean, W.H., Hahn, J.T., McRoberts, R.E., Kaisershot, D., 2013. Site index comparisons for forest species in the Upper Great Lakes Area of the United States and Canada, General Technical Report NRS-113.
Castaño-Santamaría, J., López-Sánchez, C.A., Ramón Obeso, J., Barrio-Anta, M., 2023. Development of a site form equation for predicting and mapping site quality. A case study of unmanaged beech forests in the Cantabrian range NW Spain). For. Ecol. Manag. 529, 120711 https://doi.org/10.1016/j.foreco.2022.120711.
Cieszewski, C.J., Bailey, R.L., 2000. Generalized algebraic difference approach: Theory based derivation of dynamic sire equations with polymorphism and variable asymptotes. For. Sci. 46, 116–126.
Condés, S., del Río, M., Sterba, H., 2013. Mixing effect on volume growth of Fagus sylvatica and Pinus sylvestris is modulated by stand density. For. Ecol. Manage. 292, 86–95. https://doi.org/10.1016/j.foreco.2012.12.013.
Coops, N.C., Tompalski, P., Goodbody, T.R.H., Queinnec, M., Luther, J.E., Bolton, D.K., White, J.C., Wulder, M.A., van Lier, O.R., Hermosilla, T., 2021. Modelling lidar-derived estimates of forest attributes over space and time: A review of approaches and future trends. Remote Sens. Environ. 260, 112477 https://doi.org/10.1016/j.rse.2021.112477.
Dalponte, M., Jucker, T., Liu, S., Frizzera, L., Gianelle, D., 2019. Characterizing forest carbon dynamics using multi-temporal Lidar data. Remote Sens. Environ. 224, 412–420. https://doi.org/10.1016/j.rse.2019.02.018.
Dănescu, A., Albrecht, A.T., Bauhus, J., Kohnle, U., 2017. Geocentric alternatives to site index for modeling tree increment in uneven-aged mixed stands. For. Ecol. Manage. 392, 1–12. https://doi.org/10.1016/j.foreco.2017.02.045.
del Río, M., Pretzsch, H., Alberdi, I., Bielak, K., Bravo, F., Brunner, A., Condés, S., Ducey, M.J., Fonseca, T., von Lüpke, N., Pach, M., Peric, S., Perot, T., Souidi, Z., Spathelf, P., Sterba, H., Tijardovic, M., Tomé, M., Vallet, P., Bravo-Oviedo, A., 2016. Characterization of the structure, dynamics, and productivity of mixed-species stands: review and perspectives. Eur. J. For. Res. 135, 23–49. https://doi.org/10.1007/s10342-015-0927-6.
Fekety, P.A., Falkowski, M.J., Hudak, A.T., 2015. Temporal transferability of LiDAR-based imputation of forest inventory attributes. Can. J. For. Res. 45, 422–435. https://doi.org/10.1139/cjfr-2014-0405.
Garber, S.M., Maguire, D.A., 2004. Stand productivity and development in two mixed-species spacing trials in the central Oregon cascades. For. Sci. 50, 92–105.
García, O., 1983. A stochastic differential equation model for the height growth of forest stands. Biometrics 39, 1059–1072.
García, O., 2011. Dynamical implications of the variability representation in site-index modelling. Eur. J. For. Res. 130, 671–675. https://doi.org/10.1007/s10342-010-0458-0.
García, O., 2019. Estimating reducible stochastic differential equations by conversion to a least-squares problem. Comput. Stat. 34, 23–46. https://doi.org/10.1007/s00180-018-0837-4.
Geoff Wang, G., 1998. Is height of dominant trees at a reference diameter an adequate measure of site quality? For. Ecol. Manag. 112 (1-2), 49–54.
Guerra-Hernández, J., Arellano-Pérez, S., González-Ferreiro, E., Pascual, A., Sandoval Altelarrea, V., Ruiz-González, A.D., Álvarez-González, J.G., 2021. Developing a site index model for P. Pinaster stands in NW Spain by combining bi-temporal ALS data and environmental data. For. Ecol. Manage. 481, 118690. https://doi.org/10.1016/j.foreco.2020.118690.
Hennigar, C.R., Weiskittel, A.R., Allen, H.L., Maclean, D.A., 2017. Development and evaluation of a biomass increment based index for site productivity. Can. J. For. Res. 47, 400–410. https://doi.org/10.1139/cjfr-2016-0330.
Hopkinson, C., Chasmer, L., Hall, R.J., 2008. The uncertainty in conifer plantation growth prediction from multi-temporal Lidar datasets. Remote Sens. Environ. 112, 1168–1180. https://doi.org/10.1016/j.rse.2007.07.020.
Hu, Z., García, O., 2010. A height-growth and site-index model for interior spruce in the Sub-Boreal Spruce biogeoclimatic zone of British Columbia. Can. J. For. Res. 40, 1175–1183. https://doi.org/10.1139/X10-075.
Krumland, B., Eng, H., 2005. Site index systems for major young-growth forest and woodland species in northern California. Calif. Dep. For. Fire Prot. 4, 1–220.
Lamb, S.M., MacLean, D.A., Hennigar, C.R., Pitt, D.G., 2018. Forecasting forest inventory using imputed tree lists for LiDAR grid cells and a tree-list growth model. Forests 9, 1–18. https://doi.org/10.3390/f9040167.
Maltamo, M., Vartiainen, P., Packalen, P., Korhonen, L., 2022. Estimation of periodic annual increment of tree ring widths by airborne laser scanning. Can. J. For. Res. 52, 644–651. https://doi.org/10.1139/cjfr-2021-0267.
Manso, R., McLean, J.P., Arcangeli, C., Matthews, R., 2021. Dynamic top height models for several major forest tree species in Great Britain. Forestry 94, 181–192. https://doi.org/10.1093/foresj/cpaa036.
McRoberts, R.E., Næsset, E., Gobakken, T., Bollandsås, O.M., 2015. Indirect and direct estimation of forest biomass change using forest inventory and airborne laser scanning data. Remote Sens. Environ. 164, 36–42. https://doi.org/10.1016/j.rse.2015.02.018.
Moan, M.Å., Noordermeer, L., White, J.C., Coops, N.C., Bollandsås, O.M., 2023. Detecting and excluding disturbed forest areas improves site index determination using bitemporal airborne laser. For. An Int. J. For. Res. 1–11.
Molina-Valero, J.A., Diéguez-Aranda, U., Álvarez-González, J.G., Castedo-Dorado, F., Pérez-Cruzado, C., 2019. Assessing site form as an indicator of site quality in even-aged Pinus radiata D. Don stands in north-western Spain. Ann. For. Sci. 76 https://doi.org/10.1007/s13595-019-0904-1.
Nigh, G., 2002. Site index conversion equations for mixed trembling aspen and white spruce stands in northern British Columbia. Silva Fenn. 36, 789–797. https://doi.org/10.14214/sf.521.
Nigh, G., Aravanopoulos, F.A., 2015. Engelmann spruce site index models: A comparison of model functions and parameterizations. PLoS One 10 (4), e0124079. https://doi.org/10.1371/journal.pone.0124079.
Noordermeer, L., Gobakken, T., Næsset, E., Bollandsås, O.M., 2020. Predicting and mapping site index in operational forest inventories using bitemporal airborne laser scanner data. For. Ecol. Manage. 457, 117768. https://doi.org/10.1016/j.foreco.2019.117768.
Oliver, C.D., Larson, B., 1996. Forest stand dynamics. For. Sci. 42, 397. https://doi.org/10.1093/forestscience/42.3.397.
Ontario Ministry of Natural Resources and Forestry, 2009. Forest Resources Inventory Technical Specifications.
Orrego, S., Montes, C., Restrepo, H.I., Bullock, B.P., Zapata, M., 2021. Modeling height growth for teak plantations in Colombia using the reducible stochastic differential equation approach. J. For. Res. 32, 1035–1045. https://doi.org/10.1007/s11676-020-01174-y.
Penner, M., Pitt, D., 2019. The Ontario Growth and Yield Program Status and Needs, Report to the Forestry Futures Trust Committee.
Pinheiro, J., Bates, D., 2000. Mixed-Effects Models in S and S-PLUS. Springer.
Pretzsch, H., 2020. Density and growth of forest stands revisited. Effect of the temporal scale of observation, site quality, and thinning. For. Ecol. Manage. 460, 117879. https://doi.org/10.1016/j.foreco.2020.117879.
Pretzsch, H., 2021. The social drift of trees. Consequence for growth trend detection, stand dynamics, and silviculture. Eur. J. For. Res. 140, 703–719. https://doi.org/10.1007/s10342-020-01351-y.
Pretzsch, H., Zenner, E.K., 2017. Toward managing mixed-species stands: from parametrization to prescription. For. Ecosyst. 4, 19. https://doi.org/10.1186/s40663-017-0105-z.
Pretzsch, H., 2009. Forest Dynamics, Growth and Yield. Springer Berlin Heidelberg, Berlin, Heidelberg. https://doi.org/10.1007/978-3-540-88307-4.
Puliti, S., McLean, J.P., Cattaneo, N., Fischer, C., Astrup, R., 2022. Tree height-growth trajectory estimation using uni-temporal UAV laser scanning data and deep learning. For. An Int. J. For. Res. 1–12. https://doi.org/10.1093/forestry/cpac026.
Queinnec, M., Coops, N.C., White, J.C., Griess, V.C., Schwartz, N.B., McCartney, G., 2022. Mapping dominant boreal tree species groups by combining area-based and individual tree crown LiDAR metrics with Sentinel-2 data. Can. J. Remote Sens. 1–19. https://doi.org/10.1080/07038992.2022.2130742.
Rennolls, K., 1978. "Top height"; Its definition and estiomation. Commonw. For. Rev. 57, 215–219.
Rennolls, K., 1995. Forest height growth modelling. For. Ecol. Manage. 71, 217–225. https://doi.org/10.1016/0378-1127(94)06102-O.
Riofrío, J., White, J.C., Tompalski, P., Coops, N.C., Wulder, M.A., 2022. Harmonizing multi-temporal airborne laser scanning point clouds to derive periodic annual height increments in temperate mixedwood forests. Can. J. For. Res. 52 (10), 1334–1352.
Roussel, J.-R., Auty, D., Coops, N.C., Tompalski, P., Goodbody, T.R.H., Meador, A.S., Bourdon, J.-F., de Boissieu, F., Achim, A., 2020. lidR: An R package for analysis of Airborne Laser Scanning (ALS) data. Remote Sens. Environ. 251, 112061. https://doi.org/10.1016/j.rse.2020.112061.
Saarela, S., Wästlund, A., Holmström, E., Mensah, A.A., Holm, S., Nilsson, M., Fridman, J., Ståhl, G., 2020. Mapping aboveground biomass and its prediction uncertainty using LiDAR and field data, accounting for tree-level allometric and LiDAR model errors. For. Ecosyst. 7 https://doi.org/10.1186/s40663-020-00245-0.
Salas, C., Stage, A.R., Robinson, A.P., 2008. Modeling effects of overstory density and competing vegetation on tree height growth. For. Sci. 54, 107–122.
Salas-Eljatib, C., 2020. Height growth–rate at a given height: A mathematical perspective for forest productivity. Ecol. Modell. 431, 109198 https://doi.org/10.1016/j.ecolmodel.2020.109198.
Salas-Eljatib, C., 2021. An approach to quantify climate–productivity relationships: an example from a widespread Nothofagus forest. Ecol. Appl. 31 https://doi.org/10.1002/eap.2285.
Sharma, M., 2021. Climate effects on jack pine and black spruce productivity in natural origin mixed stands and site index conversion equations. Trees, For People 5, 100089. https://doi.org/10.1016/j.tfp.2021.100089.
Sharma, M., 2022. Climate effects on black spruce and trembling aspen productivity in natural origin mixed stands. Forests 13 (3), 430. https://doi.org/10.3390/f13030430.
Sharma, M., Parton, J., 2019. Modelling the effects of climate on site productivity of white pine plantations. Can. J. For. Res. 49, 1289–1297. https://doi.org/10.1139/cjfr-2019-0165.
Sharma, M., Parton, J., Woods, M., Newton, P., Penner, M., Wang, J., Stinson, A., Bell, F. W., 2008. Ontario's forest growth and yield modelling program: Advances resulting from the forestry research partnership. For. Chron. 84, 694–703. https://doi.org/10.5558/tfc84694-5.
Skovsgaard, J.P., Vanclay, J.K., 2008. Forest site productivity: a review of the evolution of dendrometric concepts for even-aged stands. Forestry 81, 13–31. https://doi.org/10.1093/forestry/cpm041.
Skowronski, N.S., Clark, K.L., Gallagher, M., Birdsey, R.A., Hom, J.L., 2014. Airborne laser scanner-assisted estimation of aboveground biomass change in a temperate oak-pine forest. Remote Sens. Environ. 151, 166–174. https://doi.org/10.1016/j.rse.2013.12.015.

Socha, J., Pierzchalski, M., Bałazy, R., Ciesielski, M., 2017. Modelling top height growth and site index using repeated laser scanning data. For. Ecol. Manage. 406, 307–317. https://doi.org/10.1016/j.foreco.2017.09.039.

Socha, J., Hawryło, P., Stereńczak, K., Miścicki, S., Tymińska-Czabańska, L., Młocek, W., Gruba, P., 2020. Assessing the sensitivity of site index models developed using bi-temporal airborne laser scanning data to different top height estimates and grid cell sizes. Int. J. Appl. Earth Obs. Geoinf. 91, 102129. https://doi.org/10.1016/j.jag.2020.102129.

Solberg, S., Kvaalen, H., Puliti, S., 2019. Age-independent site index mapping with repeated single-tree airborne laser scanning. Scand. J. For. Res. 34, 763–770. https://doi.org/10.1080/02827581.2019.1616814.

Stepper, C., Straub, C., Pretzsch, H., 2014. Assessing height changes in a highly structured forest using regularly acquired aerial image data. Forestry 88, 304–316. https://doi.org/10.1093/forestry/cpu050.

Toïgo, M., Vallet, P., Perot, T., Bontemps, J.-D., Piedallu, C., Courbaud, B., Canham, C., 2015. Overyielding in mixed forests decreases with site productivity. J. Ecol. 103 (2), 502–512. https://doi.org/10.1111/1365-2745.12353.

Tompalski, P., Coops, N.C., White, J.C., Wulder, M.A., Pickell, P.D., 2015. Estimating forest site productivity using airborne laser scanning data and Landsat time series. Can. J. Remote Sens. 41, 232–245. https://doi.org/10.1080/07038992.2015.1068686.

Tompalski, P., Coops, N.C., White, J.C., Wulder, M.A., 2016. Enhancing forest growth and yield predictions with airborne laser scanning data: Increasing spatial detail and optimizing yield curve selection through template matching. Forests 7, 1–20. https://doi.org/10.3390/f7110255.

Tompalski, P., Rakofsky, J., Coops, N.C., White, J.C., Graham, A.N.V., Rosychuk, K., 2019. Challenges of multi-temporal and multi-sensor forest growth analyses in a highly disturbed boreal mixedwood forests. Remote Sens. 11 (18), 2102. https://doi.org/10.3390/rs11182102.

Tompalski, P., Coops, N.C., White, J.C., Goodbody, T.R.H., Hennigar, C.R., Wulder, M.A., Socha, J., Woods, M., 2021. Estimating changes in forest attributes and enhancing growth projections: a review of existing approaches and future directions using airborne 3D point cloud data. Curr. For. Reports 7, 25–30. https://doi.org/10.1007/s40725-021-00139-6.

Tompalski, P., Coops, N.C., Achim, A., Cosgrove, C.F., Lapointe, E., Brochu-Marier, F., 2022. Modeling site index of selected poplar clones using airborne laser scanning data. Can. J. For. Res. 1097, 1088–1097. https://doi.org/10.1139/cjfr-2021-0257.

Tymińska-Czabańska, L., Socha, J., Hawryło, P., Bałazy, R., Ciesielski, M., Grabska-Szwagrzyk, E., Netzel, P., 2021. Weather-sensitive height growth modelling of Norway spruce using repeated airborne laser scanning data. Agric. For. Meteorol. 308–309, 108568 https://doi.org/10.1016/j.agrformet.2021.108568.

Vanclay, J.K., Henry, N.B., 1988. Assessing site productivity of indigenous cypress pine forest in southern Queensland. Commonw. For. Rev. 67, 53–64.

Véga, C., St-Onge, B., 2009. Mapping site index and age by linking a time series of canopy height models with growth curves. For. Ecol. Manage. 257, 951–959. https://doi.org/10.1016/j.foreco.2008.10.029.

Weiskittel, A.R., Hann, D.W., Kershaw, J.A., Vanclay, J.K., 2011. Forest Growth and Yield Modeling. John Wiley & Sons.

White, J.C., Coops, N.C., Wulder, M.A., Vastaranta, M., Hilker, T., Tompalski, P., 2016. Remote sensing technologies for enhancing forest inventories: A review. Can. J. Remote Sens. 42, 619–641. https://doi.org/10.1080/07038992.2016.1207484.

White, J.C., Chen, H., Woods, M., Low, B., Nasonova, S., 2019. The petawawa research forest: Establishment of a remote sensing supersite. For. Chron. 95, 149–156. https://doi.org/10.5558/tfc2019-024.

White, J.C., Wulder, M.A., Varhola, A., Vastaranta, M., Coops, N.C., Cook, B.D., Pitt, D., Woods, M., 2013. A best practices guide for generating forest inventory attributes from airborne laser scanning data using an area-based approach, Information Report FI-X-10. Victoria, BC. https://doi.org/10.5558/tfc2013-132.

White, J.C., Tompalski, P., Vastaranta, M., Wulder, M.A., Stepper, C., Ninni, S., Coops, N. C., 2017. A model development and application guide for generating an enhanced forest inventory using airborne laser scanning data and an area-based approach, Information Report FI-X-018. Victoria, Canada.

White, J.C., Penner, M., Woods, M., 2021a. Assessing single photon LiDAR for operational implementation of an enhanced forest inventory in diverse mixedwood forests. For. Chron. 97, 78–96. https://doi.org/10.5558/tfc2021-009.

White, J.C., Woods, M., Krahn, T., Papasodoro, C., Bélanger, D., Onafrychuk, C., Sinclair, I., 2021b. Evaluating the capacity of single photon LIDAR for terrain characterization under a range of forest conditions. Remote Sens. Environ. 252, 112169. https://doi.org/10.1016/j.rse.2020.112169.

Zhao, K., Suarez, J.C., Garcia, M., Hu, T., Wang, C., Londo, A., 2018. Utility of multitemporal LIDAR for forest and carbon monitoring: Tree growth, biomass dynamics, and carbon flux. Remote Sens. Environ. 204, 883–897. https://doi.org/10.1016/j.rse.2017.09.007.

Zhou, M., Lei, X., Duan, G., Lu, J., Zhang, H., 2019. The effect of the calculation method, plot size, and stand density on the top height estimation in natural spruce-fir-broadleaf mixed forests. For. Ecol. Manage. 453, 117574 https://doi.org/10.1016/j.foreco.2019.117574.